



# The Coronary Artery Running Pattern is One of the Causes of Individual Differences in the Progression of Coronary Atherosclerosis in WHHLMI Rabbits, an Animal Model for Coronary...

Nagasaka, Ryosuke

Koike, Tomonari

Tsukada, Node

Tamura, Shohei

Shiomi, Masashi

---

## (Citation)

Journal of Atherosclerosis and Thrombosis, 25(5):393-404

## (Issue Date)

2018-05

## (Resource Type)

journal article

## (Version)

Version of Record

## (Rights)

©2018 Japan Atherosclerosis Society.

This article is distributed under the terms of the latest version of CC BY-NC-SA defined by the Creative Commons Attribution License.

## (URL)

<https://hdl.handle.net/20.500.14094/90004943>





# The Coronary Artery Running Pattern is One of the Causes of Individual Differences in the Progression of Coronary Atherosclerosis in WHHLMI Rabbits, an Animal Model for Coronary Atherosclerosis

Ryosuke Nagasaka<sup>1</sup>, Tomonari Koike<sup>2</sup>, Norie Tsukada<sup>1</sup>, Shohei Tamura<sup>1</sup> and Masashi Shiomi<sup>1,2</sup>

<sup>1</sup>Division of Comparative Pathophysiology, Kobe University Graduate School of Medicine, Kobe, Japan

<sup>2</sup>Institute for Experimental Animals, Kobe University Graduate School of Medicine, Kobe, Japan

**Aims:** The relationship between the coronary artery running pattern and development of coronary lesions was re-examined herein using WHHLMI rabbits, an animal model of spontaneous coronary atherosclerosis.

**Methods:** The coronary artery running pattern was analyzed using an X-ray computed tomography (CT) apparatus after perfusion. Pathological sections were prepared (Victoria blue-HE staining) at 100  $\mu$ m intervals from the origin of the left circumflex artery (LCX). The severity of coronary lesions was evaluated based on cross-sectional narrowing (lesion area/inner area of the internal elastic lamina).

**Results:** In the CT analysis, the angle of the main curvature of the LCX negatively correlated with the percentage of sections with lesions and cross-sectional narrowing. The percentage of sections with lesions was significantly higher in acute angle-type LCX than in obtuse angle-type LCX. Cross-sectional narrowing was also significantly greater in acute angle-type LCX than in obtuse angle-type LCX. The percentage of fibrous lesions was high at the proximal region of LCX, whereas that of lipid-rich lesions was high at the curvature. In 24 months age group, the percentage of sections with calcification in acute angle-type LCX was about twice that in obtuse angle-type LCX.

**Conclusions:** Individual differences were observed in the angle of the main curvature of the LCX, which affected the occurrence and extension of atherosclerotic lesions.

**Key words:** Coronary lesion, Coronary artery running pattern, Angle of curvature of left circumflex artery, WHHLMI rabbit

Copyright©2018 Japan Atherosclerosis Society

This article is distributed under the terms of the latest version of CC BY-NC-SA defined by the Creative Commons Attribution License.

## Introduction

Coronary atherosclerotic lesions develop diffusely and serial cross-sectional narrowing is frequently observed in humans<sup>1</sup>. These coronary lesions progress silently until the onset of coronary events. Many studies have reported that coronary lesions are responsible for cardiac events. Clinical studies using computed tomography (CT) angiography, quantitative coronary angiography, and intravascular ultrasound have frequently

detected atherosclerotic lesions at the bifurcation or curvature of coronary arteries<sup>2-6</sup>. Blood flow was found to be disturbed in these areas, and arterial wall shear stress was low and oscillated<sup>5, 7</sup>. Seneviratne *et al.*<sup>8</sup> reviewed the relationship between changes in arterial wall shear stress and plaque development and destabilization. As described above, prevalent sites of coronary lesions have been analyzed in detail. The findings obtained suggest that the coronary artery running pattern is important in the development of coronary lesions; however, limited information is available on this relationship.

We previously reported that other factors than serum cholesterol levels may be related to the progression and composition of coronary lesions in WHHLMI rabbits<sup>9</sup>. The WHHLMI rabbit is an animal model

Address for correspondence: Masashi Shiomi, Institute for Experimental Animals, Kobe University Graduate School of Medicine, 7-5-1, Kusunoki-cho, Chuo-ku, Kobe 650-0017, Japan  
E-mail: ieakusm@med.kobe-u.ac.jp

Received: June 28, 2017

Accepted for publication: September 24, 2017

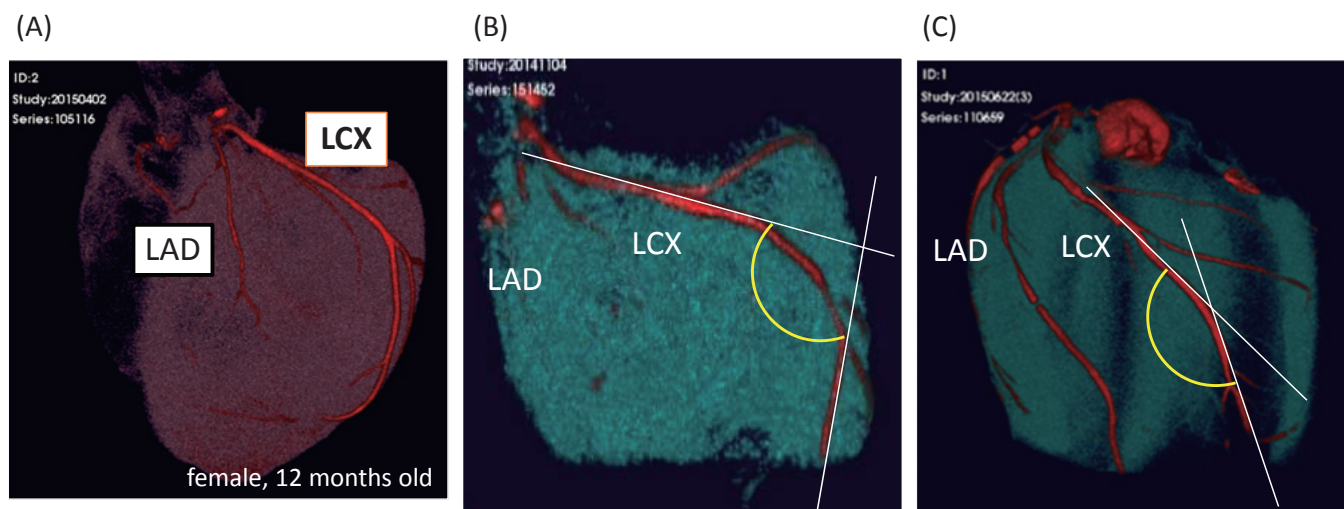


**Fig. 1.** Reconstructed CT images of the heart of a WHHLM rabbit (A) and method of measuring the angle of the LCX curved portion of acute angle-type LCX (B) and obtuse angle-type LCX (C).

In measurement of angle of LCX curvature (panels B and C), a CT reconstructed image with the apex at the bottom and the LAD at the left end was used. Tangent lines (white lines) were drawn along the straight part at the proximal and distal regions of the curvature, and the angle of the intersection point (yellow curve lines) of the tangent lines was measured. LAD, left anterior descending artery; LCX, left circumflex artery

for human familial hypercholesterolemia<sup>10</sup>) and develops diffuse coronary lesions<sup>9,11</sup>) even with normal chow feeding. The factors responsible for individual differences in the development of coronary lesions have yet to be identified. Furthermore, individual differences in coronary artery running patterns have not been examined, and it currently remains unclear whether these individual differences affect the severity of coronary lesions. Therefore, we herein investigated whether the coronary artery running pattern on the surface of the left ventricular wall is related to the progression and composition of atherosclerotic lesions.

## Materials and Methods

### Animals

Five WHHLM rabbits (3 females and 2 males) aged approximately 6 months (5–7 months old), 8 WHHLM rabbits (7 females and 1 male) aged approximately 12 months (12–13 months old), and 6 WHHLM rabbits (3 females and 3 males) aged approximately 24 months (23–25 months old) were used in the present study. WHHLM rabbits were bred at the Institute for Experimental Animals, Kobe University Graduate School of Medicine. Rabbits were housed individually in metal cages (550 × 600 × 450 mm; in width, depth, and height, respectively) with a flat metal floor and fed standard rabbit chow (LRC4, Oriental Yeast Co., Ltd., Tokyo, Japan) at 120 g/day and water *ad libitum*. Animals were maintained under SPF

conditions at a constant temperature ( $22 \pm 2^\circ\text{C}$ ), relative humidity (50%–60%), ventilation rate (15 cycles/hour), air supply (through the HEPA filter), and lighting cycle (12 hours light/dark). This study was approved by the Kobe University Animal Care and Use Committee (approval numbers: P140406 and P140801), and all animal experiments were conducted in accordance with the Regulations for Animal Experimentation of Kobe University, the Act on Welfare and Management of Animals (Law No. 105, 1973, revised in 2006), Standards Relating to the Care and Management of Laboratory Animals and Relief of Pain (Notification No. 88, 2006), and Fundamental Guidelines for the Proper Conduct of Animal experiments and Related Activities in Academic Research Institutions under the Jurisdiction of the Ministry of Education, Culture, Sports, Science and Technology (Notice No. 71, 2006).

### Analyses of the Running Pattern of the Left Circumflex Artery (LCX) with an X-ray Micro CT Imager

Hearts were excised from rabbits euthanized with an intravenous injection of pentobarbital. Hearts were then perfused with saline followed by 10% buffered neutral formalin solution. Coronary arteries were injected with the contrast medium, Microfil silicone rubber injection compound (Flow Tech Inc., South Windsor, CT, USA). Coronary artery running patterns were evaluated with the 3 dimensional X-ray micro CT imagers, R\_mCT2 (Rigaku Co., Tokyo, Japan), and images

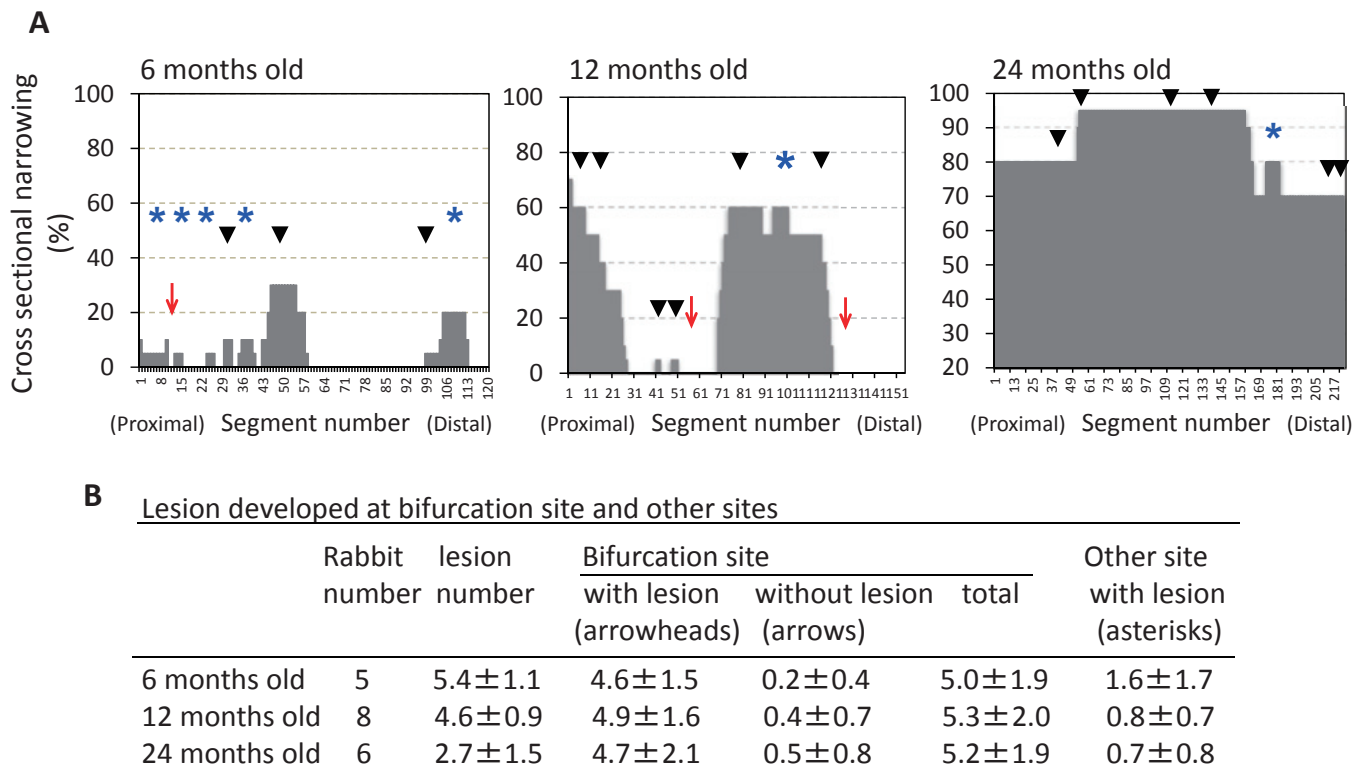


**Fig. 2.** Distribution of atherosclerotic lesions in left circumflex artery (LCX) of WHHLMi rabbits aged 6, 12, or 24 months.

(A) Figures demonstrate a representative rabbit in each age group with lesions developed at both bifurcation and non-bifurcation sites. Asterisks indicate non-bifurcation site with lesions. Arrowheads indicate bifurcation site with lesions. Arrows indicate the bifurcation site without lesions. (B) Summary of the site where the lesion occurred. The number of lesions were counted as the peak on cross-sectional narrowing. Data are represented as the mean ± SD.

were reconstructed with the software, 3D Viewer (Rigaku Co., Tokyo, Japan). The X-ray source was set to a current of 160  $\mu$ A and voltage of 90 kV. The scan time was set to 2 or 3 min. The field of view was set to 24 × 24 mm or 30 × 30 mm, and the voxel size was set to 50 or 59  $\mu$ m. We analyzed the LCX because this vessel in WHHLMi rabbits has a greater diameter and length than those of the left anterior descending artery (LAD) (**Fig. 1**), and atherosclerotic lesions develop more frequently in the LCX than in the LAD in WHHLMi rabbits<sup>12, 13</sup>. We measured the angle of curvature from the basis cordis parallel direction to the apical direction, using the digital photograph of the CT reconstructed images with the apex at the bottom and the LAD at the left end was used for analysis (**Fig. 1**). Tangent lines were drawn along the straight part at the proximal and distal regions of the LCX curvature on the digital photographs of the CT reconstructed images, and the angle of intersection point of the tangent lines was measured. We analyzed the relationship between the angle of curvature and the atherosclerotic lesion.

### Preparation of Coronary Sections

After the evaluation of coronary artery running patterns, coronary sections were prepared as reported previously<sup>14</sup>. Each LCX segment was sliced at 100  $\mu$ m intervals and ten 4  $\mu$ m thick serial sections were prepared from the proximal to midpoint between the basis cordis and apex. Coronary sections were prepared from 138 ± 22 (mean ± the standard deviation) segments from rabbits in the 6 months old group, 169 ± 12 segments from rabbits in the 12 months old group, and 193 ± 31 segments from rabbits in the 24 months old group. Sections were stained immunohistochemically with monoclonal antibodies: RAM-11 (Dako A/S, Glostrup, Denmark), specific for rabbit macrophages/macrophage-derived foam cells<sup>15</sup>, and 1A4 (Dako A/S), specific for the alpha-actin of smooth muscle cells (SMC), in addition to Victoria blue-HE staining. The severity of coronary lesions was evaluated as cross-sectional narrowing calculated by dividing lesion area with the area of lesions and lumen. The location of the coronary sections in the heart was determined by comparing the position of branches on

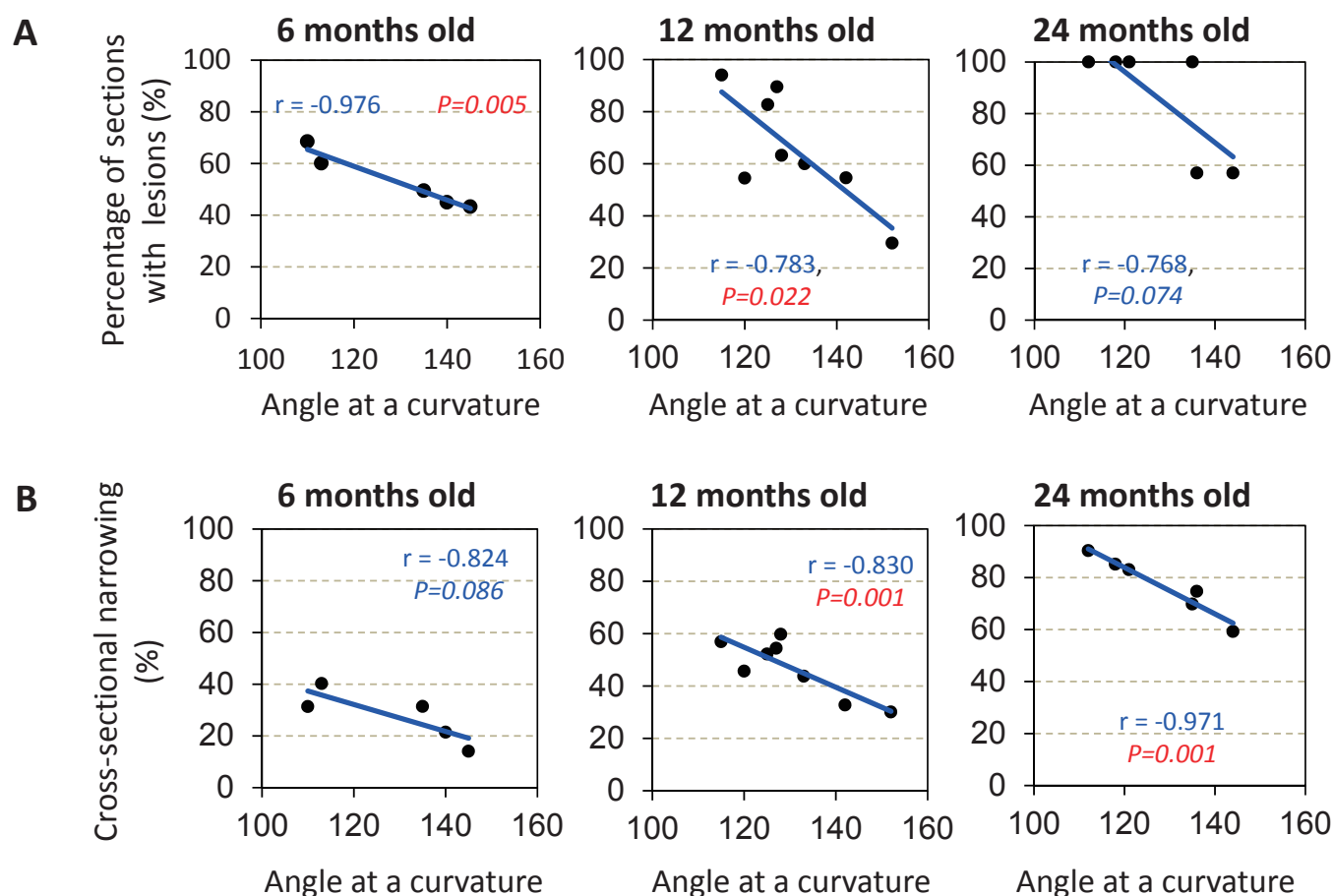


**Fig. 3.** Relationship between angle at LCX curvature and coronary lesions in WHHLMi rabbits.

(A) Correlation analyses between the angle of the curvature of the LCX and the percentage of sections with lesion. (B) Correlation analyses between the angle of the curvature of the LCX and cross-sectional narrowing. The correlation coefficient was calculated by Pearson's method.

the reconstructed CT image with the location of branches observed in the histopathological sections.

### Classification of Coronary Lesions

In the present study, coronary lesions were classified to fibrous lesion, combined lesion, macrophage-rich lesion, and plaque with necrotic core. We classified lesions as follows: 1) lesions in which SMC, collagen fibers, and elastic fibers occupy 80% or more of the intimal lesion was defined as fibrous lesions; 2) lesions in which fibrous component and lipids/macrophages were layered were classified as combined lesions; 3) lesions in which RAM-11-positive cells (macrophages or macrophage-derived foam cells) occupied 1/3 or more of plaque area was classified as macrophage-rich lesions; 4) lesions with necrotic or lipid core were classified as plaque with lipid core; 5) macrophage-rich lesions and plaques with lipid cores were collectively classified as lipid-rich lesion. In addition,

we also observed coronary artery calcification using sections stained by Victoria blue-HE staining and Dahl staining.

### Other Assays

After more than 12 hours of fasting, total cholesterol and triglyceride levels in serum were assayed with dry chemistry using Fuji Dri-Chem 3500SV (Fuji Film Co. Ltd., Tokyo, Japan)<sup>16</sup>.

### Statistical Analyses

Data are represented as the mean  $\pm$  standard deviation (SD). Statistical analyses were performed on mean values using the Mann-Whitney *U*-test or Student's *t*-test. Multiple comparison tests were performed using Steel-Dwass test. Correlation analyses were performed with Pearson's correlation analysis. *P*-values less than 0.05 were considered to be significant.



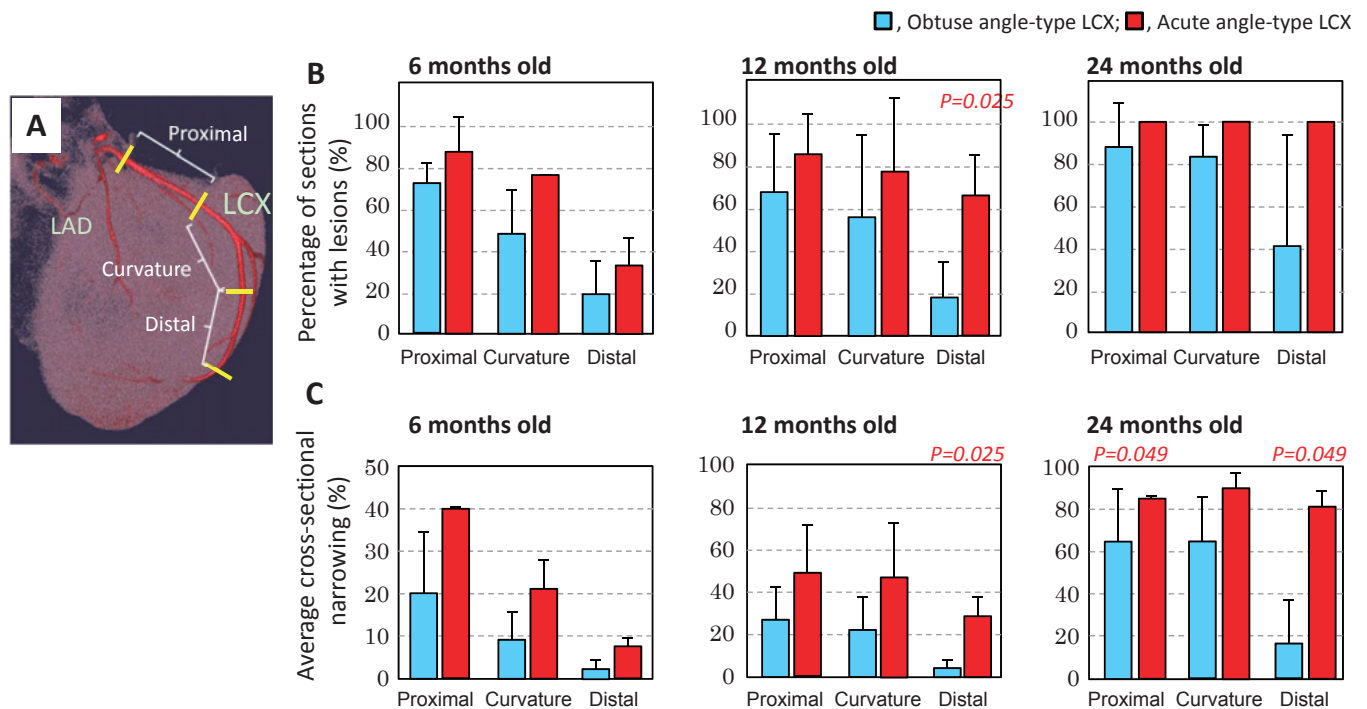


**Fig. 4.** Development of coronary lesions at the proximal site, curvature, and distal site of obtuse angle-type and acute angle-type LCX.

(A) Reconstructed CT image of the heart of a WHHLM rabbit showing the examined area. (B) Percentage of sections with lesions at the proximal, curvature, and distal regions of the LCX. (C) The mean value of coronary cross-sectional narrowing at the proximal, curvature, and distal regions of the LCX. In 6 months old group, number of rabbits was 3 in obtuse angle-type and 2 in acute angle-type. In 12 months old group, number of rabbits was 5 in obtuse angle-type LCX and 3 in acute angle-type LCX. In 24 months-old group, number of rabbits was 3 in both obtuse and acute angle-type LCX. Data are represented as the mean  $\pm$  SD. Statistical analyses were performed by Mann–Whitney U-test.

## Results

### Background Data of WHHLM Rabbits

**Supplemental Table 1** shows background data of WHHLM rabbits used in this study. Each rabbit had hypercholesterolemia. The severity (cross-sectional narrowing) and percentage of coronary sections with lesions increased with aging. We used both genders in this study. Serum total cholesterol levels were higher in males, whereas there were no gender differences in the severity of coronary lesions except rabbits in 6 months old group.

### Distribution of Atherosclerotic Lesions in the LCX

**Fig. 2** shows cross-sectional narrowing of the LCX from the origin to the midpoint between the basis cordis and apex. The number of lesions was counted as the number of peaks on cross-sectional narrowing. A large number of lesions were observed at the bifurcation (arrowheads) and some lesions developed at non-branching sites (asterisks). However, some branching sites did not have lesions (arrows).

### Diversity in LCX Running Pattern Visualized with CT Images

LCX running patterns were very diverse (**Fig. 1**), and the angle of curvature was negatively associated with the percentage of sections with lesions [ $r = -0.976$ ,  $P = 0.005$  in 6 months old group;  $r = -0.783$ ,  $P = 0.022$  in 12 months old group; and  $r = -0.768$ ,  $P = 0.074$  in 24 months old (**Fig. 3A**)], and average of cross-sectional narrowing [ $r = -0.824$ ,  $P = 0.086$  in 6 months old group;  $r = -0.830$ ,  $P = 0.001$  in 12 months old group;  $r = -0.971$ ,  $P = 0.001$  in 24 months old group (**Fig. 3B**)]. The angle at curvature of the LCX ranged between 100 to 152 degrees [ $129 \pm 13$  degrees ( $n = 19$ )]. The first quartile was 118, the second quartile was 128, and the third quartile was 140. No significant gender differences were observed in the curvature angle of the LCX. LCX curvature angle 130 degrees was chosen for classification of obtuse and acute angle-type LCX, because the mean value for this angle was 129 degrees. The percentage of sections with lesions was 18%–29% higher in acute angle-type LCX than in obtuse angle-type LCX in each age group (**Supplemental Fig. 1**),

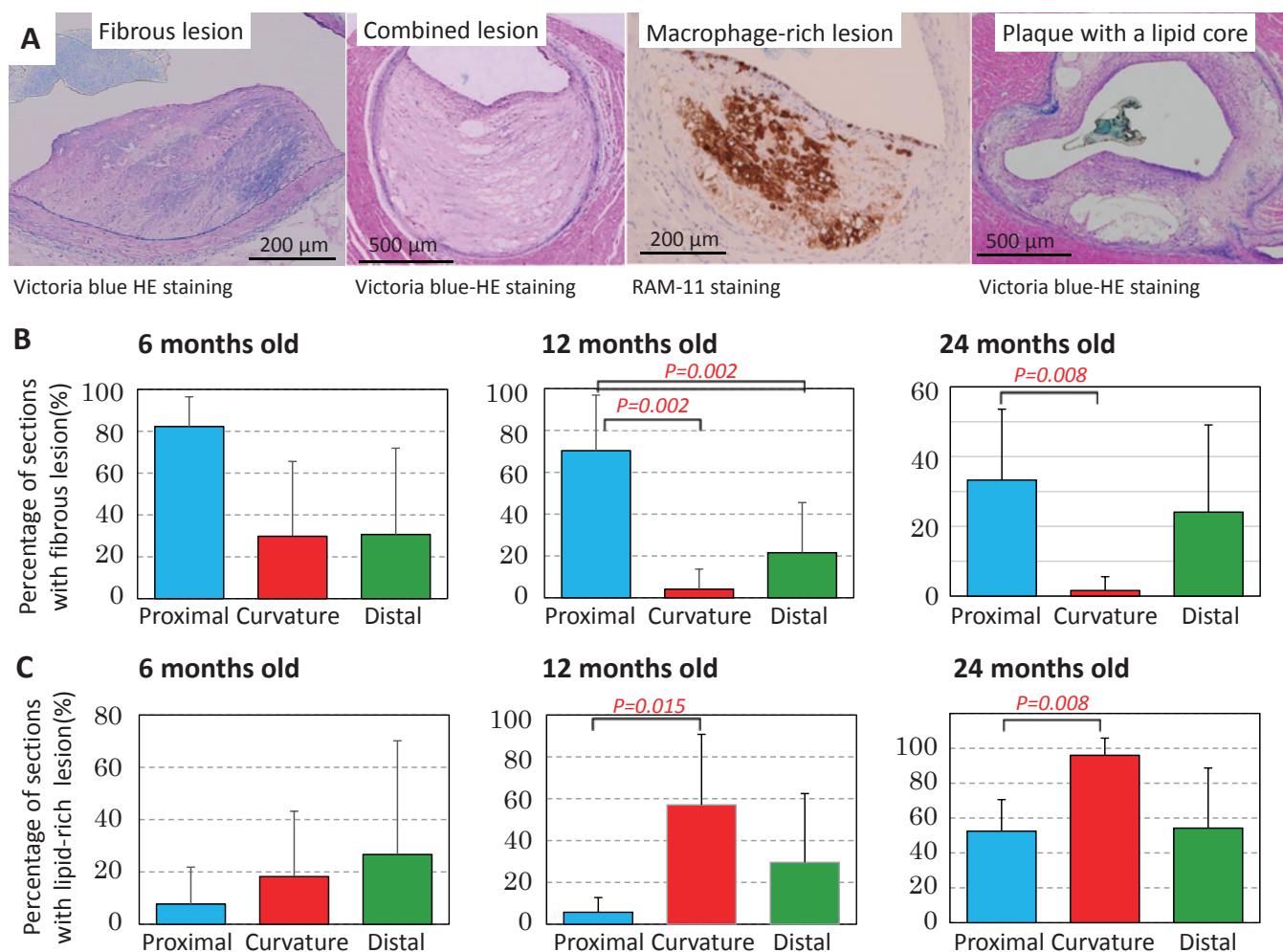


**Fig. 5.** Photomicrographs of coronary lesions and percentage of sections showing each type of lesions.

(A) Photomicrographs of coronary lesions in WHHLMI rabbits. (B) Percentage of sections with fibrous lesions at the proximal, curvature and distal regions of LCX. (C) Percentage of sections with lipid-rich lesions (macrophage-rich lesions + plaques with lipid cores) at the proximal, curvature and distal regions of LCX. Number of rabbits was 5 in 6 months-old group, 8 in 12 months-old group, and 6 in 24 months-old group. Data are represented as the mean  $\pm$  SD. Statistical analyses were performed by Steel-Dwass test.

although there was no statistical significance. The average of cross-sectional narrowing of LCX was significantly higher in acute angle-type LCX than in obtuse angle-type LCX in 12 months old [ $54 \pm 5$  ( $n=5$ ) vs.  $36 \pm 7$  ( $n=3$ ),  $P=0.025$ ] and 24 months old [ $86 \pm 4$  ( $n=3$ ) vs.  $68 \pm 8$  ( $n=3$ ),  $P=0.049$ ] (**Supplemental Fig. 1**).

#### Atherosclerotic Lesions at Proximal, Curved, and Distal Regions of the LCX

For the LCX curved part (5,000 to 8,000  $\mu$ m) and the adjacent proximal and distal regions of the same length, coronary lesions were examined using histopathological sections (**Fig. 4A**). The LCX curved part in the histopathological sections was specified by the location of branches and the shape of coronary artery, comparing with the CT images. Coronary lesions were

the most prevalent at the proximal region, followed by the curvature and distal region. The percentage of sections with lesions was higher in acute angle-type LCX than in obtuse angle-type LCX (**Fig. 4B**). Compared to the obtuse angle-type LCX, the percentage at the curvature of acute angle-type LCX was remarkably high at the 6 months old [ $77 \pm 0\%$  ( $n=2$ ) vs.  $49 \pm 21\%$  ( $n=3$ )] and the percentage at the distal region of 12 months old groups [ $66 \pm 19\%$  ( $n=5$ ) vs.  $19 \pm 16\%$  ( $n=3$ ),  $P=0.025$ ]. Cross-sectional narrowing was significantly greater in acute angle-type LCX than obtuse angle-type LCX [ $29 \pm 9\%$  ( $n=5$ ) vs.  $4 \pm 4\%$  ( $n=3$ ),  $P=0.025$ , in the distal region of 12 months old group;  $85 \pm 1\%$  ( $n=3$ ) vs.  $65 \pm 25\%$  ( $n=3$ ),  $P=0.049$ , in the proximal region of 24 months old; and  $83 \pm 7\%$  ( $n=3$ ) vs.  $16 \pm 22\%$  ( $n=3$ ),  $P=0.049$ , in the distal region of

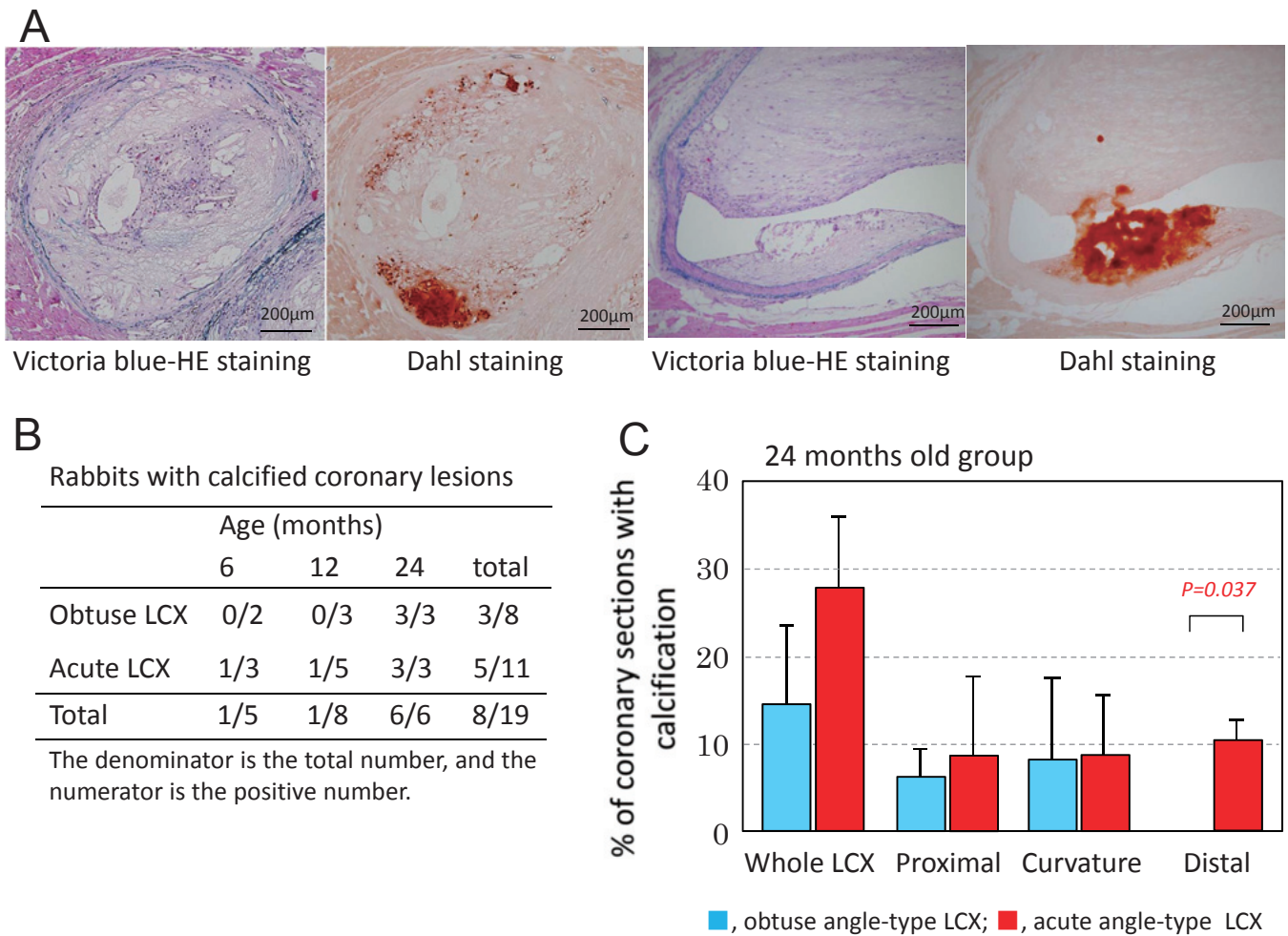


**Fig. 6.** Coronary artery calcification in the left circumflex artery.

(A) Photomicrographs of coronary artery calcification in WHHLMi rabbits. Calcification was observed not only in the deep area of coronary lesions (the left side) but the plaque surface (the right side). (B) The frequency of rabbits with coronary calcification. (C) Percentage of coronary sections with calcification. Number of rabbits was 3 in both obtuse angle-type LCX and acute angle-type LCX. Data are represented as the mean  $\pm$  SD. Statistical analyses were performed by Mann–Whitney *U*-test.

24 months old] (**Fig. 4C**).

#### Relationship between Lesion Type and Lesion Site

**Fig. 5** shows relationship between lesion type and lesion site in the LCX of WHHLMi rabbits. Fibrous lesions, combined lesions, macrophage-rich lesions, and plaques with lipid cores were observed in the LCX of WHHLMi rabbits (**Fig. 5A**). Fibrous lesions were observed frequently at the proximal region of LCX (**Fig. 5B**). The percentage of sections with fibrous lesions was significantly higher at the proximal region than at the curvature [ $70 \pm 27\%$  vs.  $4 \pm 10\%$ ,  $P=0.002$  in 12 months old group ( $n=8$ );  $33 \pm 20\%$  vs.  $2 \pm 4\%$ ,  $P=0.008$ , in 24 months old group ( $n=6$ )]. In contrast, lipid-rich lesions (macrophage-rich lesion+plaques with lipid cores) were observed frequently at the curvature of

LCX (**Fig. 5C**). The percentage of sections with lipid-rich lesions was significantly higher at the curvature than at the proximal region [ $57 \pm 34\%$  vs.  $6 \pm 7\%$ ,  $P=0.015$ , in 12 months old group ( $n=8$ );  $96 \pm 10\%$  vs.  $52 \pm 18\%$ ,  $P=0.008$ , in 24 months old group ( $n=6$ )]. In analysis using all rabbits (**Supplemental Table 2**), the percentage of sections with fibrous lesions was  $44 \pm 20\%$  in obtuse angle-type LCX ( $n=9$ ) and  $27 \pm 15\%$  in acute angle-type LCX ( $n=10$ ), whereas the percentage of sections with lipid-rich lesions was  $32 \pm 31\%$  in obtuse angle-type LCX ( $n=9$ ) and  $42 \pm 26\%$  in acute angle-type LCX ( $n=10$ ). Coronary artery calcification in LCX was observed not only in the deep area of coronary lesions but the plaque surface (**Fig. 6A**). The frequency of rabbits with coronary calcification was 20% (1/5) in the 6 months old group, 12.5% (1/8)



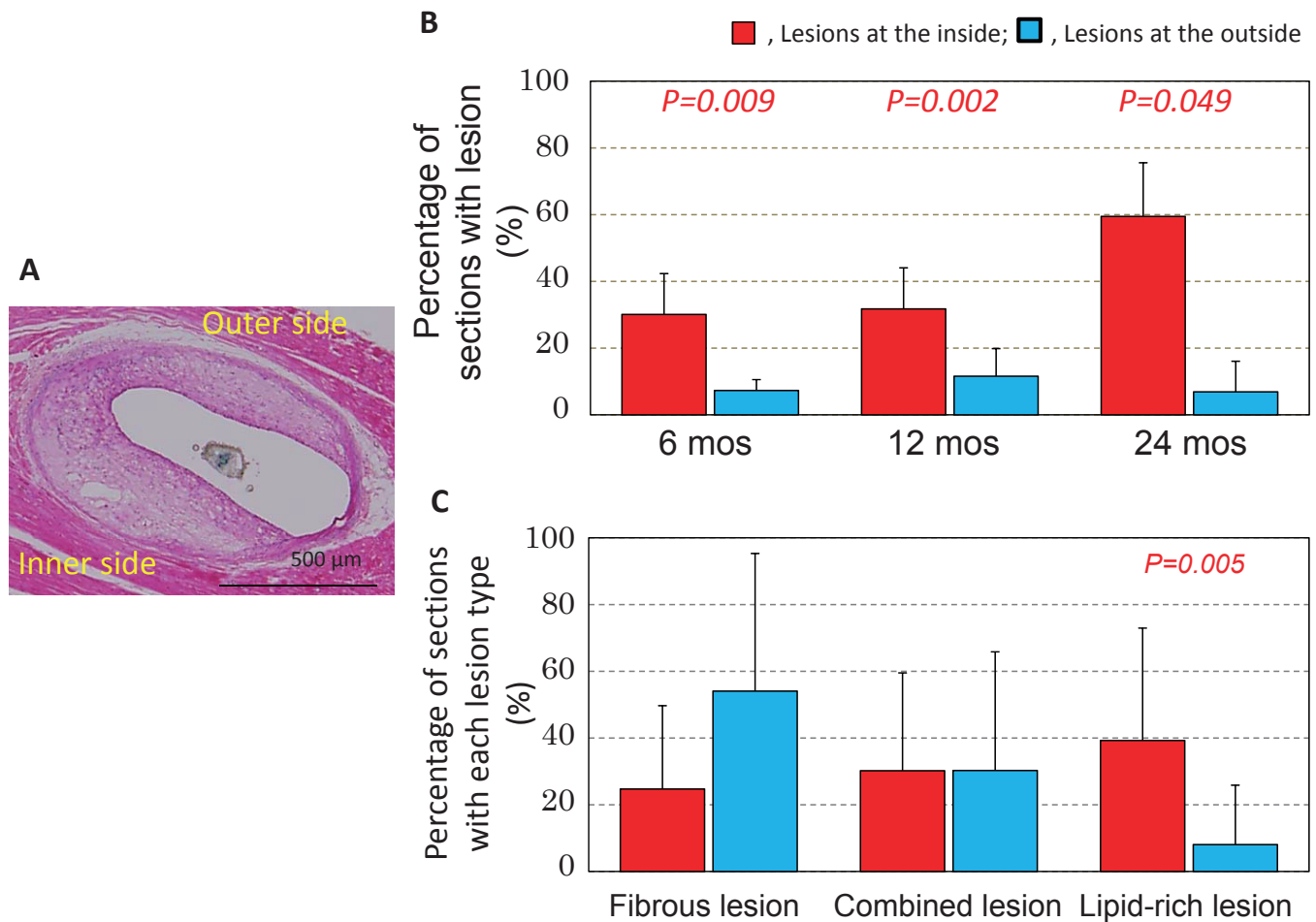


**Fig. 7.** Differences in the development of atherosclerotic lesion between inside and outside the curved area of LCX sections.

(A) A microphotograph of coronary lesions showing inside and outside the curved area of LCX sections. (B) Percentage of sections with lesions inside (red bars) or outside (blue bars) the curved area of the LCX. Number of rabbits was 5 in 6 months-old group, 8 in 12 months-old group, and 3 in 24 months-old group. (C) Percentage of sections with each type of lesions inside (red bars) or outside (blue bars) the curved area of the LCX using rabbits of all age groups. Number of rabbits was 17 in analyses of inside lesions, and 15 in analyses of outside lesions. Data are represented as the mean  $\pm$  SD. Statistical analyses were performed by Mann–Whitney *U*-test.

in the 12 months old group, and 100% (6/6) in the 24 months old group (**Fig. 6B**). Coronary calcification was observed in sections showing 60% or more cross-sectional narrowing, and most of them were observed in sections showing 90% or more cross-sectional narrowing. In 24 months old group, the percentage of sections with calcification was  $7.5 \pm 6.2\%$  in the proximal area,  $8.5 \pm 7.4\%$  in the curvature, and  $5.2 \pm 5.9\%$  in the distal area. Compared to the obtuse angle-type LCX, the percentage was about twice in the acute angle-type LCX in the whole LCX ( $27.9 \pm 8.7\%$  vs.  $14.5 \pm 9.1\%$ ), and was  $10.5 \pm 2.3\%$  in the acute angle-type LCX and 0% in the obtuse angle-type LCX ( $P=0.037$ ) at the distal region (**Fig. 6C**). There were no significant differences in serum lipid levels between obtuse angle-type LCX and acute angle-type LCX

(**Supplemental Table 2**).

#### Differences in the Development of Atherosclerotic Lesion between Inside and Outside the Curved Area of LCX Sections

Since the LCX was curved on the cardiac surface as shown in **Fig. 1**, the cross-sections of the LCX consist of inside (slow blood flow) and outside (fast blood flow) at the curvature. In addition, the ventricle side of the lumen in cross-sections is inside, whereas the epicardial side is outside because coronary arteries are located on the curved surface of cardiac wall. **Fig. 7** shows differences in the development of coronary lesions between inside and outside LCX cross-sections. The percentage of sections with lesions was statistically higher inside than outside the curved part [ $30 \pm 12\%$  vs.  $7 \pm$

3%,  $P=0.009$  at 6 months old group ( $n=5$ ),  $32 \pm 12\%$  vs.  $12 \pm 8\%$ ,  $P=0.002$  at 12 months old group ( $n=8$ ), and  $59 \pm 16\%$  vs.  $7 \pm 9\%$ ,  $P=0.049$  at 24 months old group ( $n=3$ ), (**Fig. 7B**]. The percentage of sections with fibrous lesions was  $25 \pm 25\%$  inside the curved part ( $n=17$ ) and  $54 \pm 41\%$  outside the curved part ( $n=15$ ), whereas the percentage of sections with lipid-rich lesions (**Fig. 7C**) was significantly higher inside the curved part than on the outside [ $39 \pm 34\%$  vs.  $8 \pm 18\%$ ,  $P=0.005$ ].

## Discussion

The present study using WHHLM rabbits demonstrated that the running pattern of LCX showed large individual differences, and coronary lesions progressed in acute angle-type LCX. Previous studies did not investigate whether differences in coronary artery running patterns are responsible for the development and progress of coronary lesions. Therefore, the present results provided novel insights into the development and progression of coronary lesions.

The progression of coronary lesions was more prominent in acute angle-type LCX than in obtuse angle-type LCX. Arterial wall shear stress is known to be low at the curvature and branching site, and atherosclerotic lesions are more likely to develop in these area<sup>17-21</sup>. The present results are consistent with previous findings. Furthermore, lipid-rich lesions were more prevalent inside than outside curved vessels. These results appear to support coronary lesions being more prominent in acute angle-type LCX than in obtuse angle-type LCX.

The frequency of sections with lipid-rich lesions also increased at the curvature. Similar results have been reported in humans<sup>22</sup>. In low shear stress area, arterial endothelial cells exhibit greater susceptibility to atherogenesis due to the oxidation of lipids and their accumulation in the intima<sup>23, 24</sup>. In addition, the recruitment of monocytes to the arterial intima is induced due to an increase in expression of monocyte adhesion molecule in arterial endothelial cells<sup>23</sup>. These findings support acute angle-type coronary arteries being more atherogenic than obtuse angle-type one. In the present study, coronary calcification was observed in all rabbits in 24 months old group, and was observed in LCX from proximal to distal area. Thilo *et al.*<sup>25</sup> reported that calcification was observed in a wide range of human coronary arteries by CT analysis. Since calcification was observed in sections showing 60% or more cross-sectional narrowing, and most of them were observed in sections showing 90% or more cross-sectional narrowing, progression of coronary lesion may relate to formation of calcified core. The present results

are similar to the report of CT calcium scoring on human coronary artery lesion<sup>25</sup>. In the previous studies, the coronary artery calcium score was useful for clinical applications in Japanese individuals<sup>26</sup>, and coronary artery calcium score is an independent predictor of cardiac event<sup>2</sup>. These studies suggest strongly that calcification of coronary lesions is important in destabilization of coronary plaques and occurrence of cardiac events. Galaska *et al.*<sup>4</sup> reported that the third quartile of coronary calcium score of heterozygous familial hypercholesterolemia (FH) was markedly high compared to non-FH patients with hypercholesterolemia. The authors speculated that FH genotype affects atherogenesis in coronary arteries. The information of coronary calcification of WHHLM rabbits may be helpful for future studies.

In this examination, we used a small number of rabbits. Since there is a possibility that sufficient detection power may not be obtained because the number of samples is small, it is necessary to consider further increasing the number of samples.

In conclusion, the present study using WHHLM rabbits revealed large individual differences in the angle of the main curvature of the LCX, and coronary lesions were more prevalent in acute angle-type LCX than in obtuse angle-type LCX. Furthermore, lipid-rich lesions were prevalent at the curvature of LCX. Therefore, running pattern of coronary arteries is an important factor in the development of coronary lesions.

## Financial Sources

This study was partly supported by a Grant-in-Aid for Scientific Research from the Ministry of Education, Culture, Sports and Technology, Japan (23300157 to Masashi Shiomi).

## Conflict of Interest

The authors declared they do not have anything to disclose regarding conflict of interest with respect to this manuscript.

## References

- 1) Seiler C, Kirkeeide RL, and Gould KL. Basic structure-function relations of the epicardial coronary vascular tree. Basis of quantitative coronary arteriography for diffuse coronary artery disease. *Circulation*, 1992; 85: 1987-2003
- 2) Takamura K, Fujimoto S, Kondo T, Hiki M, Kawaguchi Y, Kato E, Daida H. Incremental Prognostic Value of Coronary Computed Tomography Angiography: High-Risk Plaque Characteristics in Asymptomatic Patients. *J Atheroscler Thromb*, 2017; 24: 1174-1185
- 3) Urabe Y, Yamamoto H, Kitagawa T, Utsunomiya H, Tsu-

- shima H, Tatsugami F, Awai K, Kihara Y. Identifying Small Coronary Calcification in Non-Contrast 0.5-mm Slice Reconstruction to Diagnose Coronary Artery Disease in Patients with a Conventional Zero Coronary Artery Calcium Score. *J Atheroscler Thromb*, 2016; 23: 1324-1333
- 4) Galaska R, Kulawiak-Galaska D, Wegrzyn A, Wasag B, Chmara M, Borowiec J, Studniarek M, Fijalkowski M, Rynkiewicz A, Gruchala M. Assessment of Subclinical Atherosclerosis Using Computed Tomography Calcium Scores in Patients with Familial and Nonfamilial Hypercholesterolemia. *J Atheroscler Thromb*, 2016; 23: 588-595
  - 5) Chatzizisis YS, Toutouzas K, Giannopoulos AA, Riga M, Antoniadis AP, Fujinomi Y, Mitsouras D, Koutkias VG, Cheimariotis G, Doulaverakis C, Tsampoulatis I, Chouvarda I, Kompatsiaris I, Nakamura S, Rybicki FJ, Maglaveras N, Tousoulis D, and Giannoglou GD. Association of global and local low endothelial shear stress with high-risk plaque using intracoronary 3D optical coherence tomography: Introduction of 'shear stress score'. *Eur Hear J Cardiovasc Imaging*, 2017; 18: 888-897
  - 6) McDaniel MC, Galbraith EM, Jeroudi AM, Kashlan OR, Eshrehardi P, Suo J, Dhawan S, Voeltz M, Devireddy C, Oshinski J, Harrison DG, Giddens DP, and Samady H. Localization of culprit lesions in coronary arteries of patients with ST-segment elevation myocardial infarctions: relation to bifurcations and curvatures. *Am Heart J*, 2010; 161: 508-515
  - 7) Chen X, Gao Y, Lu B, Jia X, Zhong L, Kassab GS, Tan W, and Huo Y. Hemodynamics in coronary arterial tree of serial stenoses. *PLoS One*, 2016; 11: e0163715
  - 8) Seneviratne A, Hulsmans N, Holvoet P, and Monaco C. Biomechanical factors and macrophages in plaque stability. *Cardiovasc Res*, 2013; 99: 284-293
  - 9) Yamada S, Koike T, Nakagawa T, Kuniyoshi N, Ying Y, Itabe H, Yamashita A, Asada Y, and Shiomi M. Morphological features of coronary plaques in WHHLMi rabbits (*Oryctolagus cuniculus*), an animal model for familial hypercholesterolemia. *Exp Anim*, 2017; 79: 145-157
  - 10) Shiomi M, Ito T, Yamada S, Kawashima S, and Fan J. Development of an animal model for spontaneous myocardial infarction (WHHLMi rabbit). *Arterioscler Thromb Vasc Biol*, 2003; 23: 1239-1244
  - 11) Shiomi M, Ishida T, Kobayashi T, Kawashima S, and Fan J. Vasospasm of Atherosclerotic Coronary Arteries Precipitates Acute Ischemic Myocardial Damage in Myocardial Infarction-Prone Strain of the Watanabe Heritable Hyperlipidemic Rabbits. *Arterioscler Thromb Vasc Biol*, 2013; 33: 2518-2523
  - 12) Ito T, Yamada S, and Shiomi M. Progression of coronary atherosclerosis relates to the onset of myocardial infarction in an animal model of spontaneous myocardial infarction (WHHLMi rabbits). *Exp Anim*, 2004; 53: 339-346
  - 13) Shiomi M, Ito T, Tsukada T, Yata T, and Ueda M. Cell compositions of coronary and aortic atherosclerotic lesions differ; An immunohistochemical study. *Arterioscler Thromb*, 1994; 14: 931-937
  - 14) Shiomi M, Ito T, Shiraishi M, and Watanabe Y. Inheritability of atherosclerosis and the role of lipoproteins as risk factors in the development of atherosclerosis in WHHL rabbits: Risk factors related to coronary atherosclerosis are different from those related to aortic atherosclerosis. *Atherosclerosis*, 1992; 96: 43-52
  - 15) Tsukada T, Rosenfeld M, Ross R, and Gown AM. Immunocytochemical analysis of cellular components in atherosclerotic lesions, use of monoclonal antibodies with the Watanabe and fat-fed rabbit. *Arteriosclerosis*, 1986; 6: 601-613
  - 16) Yamada S, Ito T, Tamura T, and Shiomi M. Age-related changes in serum/plasma biochemical parameters of WHHLMi rabbits. *Exp Anim*, 2004; 53: 159-163
  - 17) Li MX, Beech-Brandt JJ, John LR, Hoskins PR, and Eason WJ. Numerical analysis of pulsatile blood flow and vessel wall mechanics in different degrees of stenoses. *J Biomech*, 2007; 40: 3715-3724
  - 18) Enrico B, Suranyi P, Thilo C, Bonomo L, Costello P, and Schoepf UJ. Coronary artery plaque formation at coronary CT angiography: morphological analysis and relationship to hemodynamics. *Eur Radiol*, 2009; 19: 837-844
  - 19) Caro CG, Fitz-Gerald JM, and Schroter RC. Atheroma and arterial wall shear. Observation, correlation and proposal of shear dependent mass transfer mechanism for atherogenesis. *Proc R Soc Lond Biol Sci*, 1971; 117: 109-159
  - 20) Friedman MH, Hutchins GM, Barger CB, Deters OJ, and Mark FF. Correlation of human arterial morphology with hemodynamic measurements in arterial casts. *J Biomech Eng*, 1981; 103: 204-207
  - 21) Siegel JM, Markou CP, Ku DN, and Hanson SR. A scaling law for wall shear stress rate through an arterial stenosis. *J Biomech Eng*, 1994; 116: 446-451
  - 22) Slager CJ, Wentzel JJ, Gijzen FJH, Schuurbers JCH, van der Wal AC, van der Steen AF, and Serruys PW. The role of shear stress in the generation of rupture-prone vulnerable plaques. *Nat Clin Pract Cardiovasc Med*, 2005; 2: 401-407
  - 23) Malek AM, Alper SL, and Izumo S. Hemodynamic shear stress and its role in atherosclerosis. *JAMA*, 1999; 282: 2035-2042
  - 24) Kinlay S, Libby P, and Ganz P. Endothelial function and coronary artery disease. *Curr Opin Lipidol*, 2001; 12: 383-389
  - 25) Thilo C, Gebregziabher M, Mayer FB, Zwerner PL, Costello P, Schoepf UJ. Correlation of regional distribution and morphological pattern of calcification at CT coronary artery calcium scoring with non-calcified plaque formation and stenosis. *Eur Radiol*, 2010; 20: 855-861
  - 26) Yamamoto H, Kitagawa T, Kihara Y. Clinical implications of the coronary artery calcium score in Japanese patients. *J Atheroscler Thromb*, 2014; 21: 1101-1108

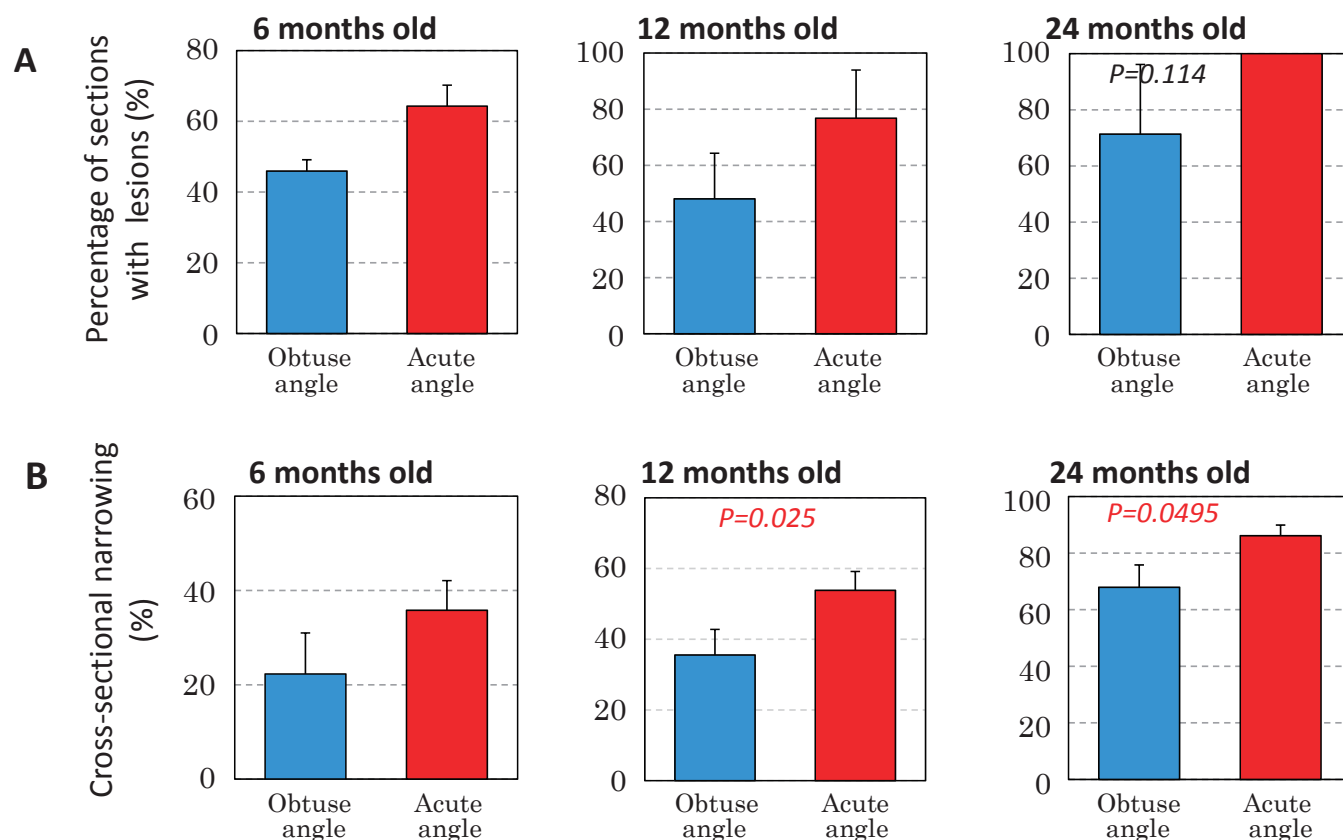
**Supplemental Table 1.** Characteristics of WHHLMI rabbits used in this study.

	6 months old group		12 months old group		24 months old group	
	Female	Male	Female	Male	Female	Male
Number of rabbits used in this study	3	2	7	1	3	3
Serum lipid levels (mmol/l) at 2 months old	(n=3)	(n=2)	(n=7)	(n=1)	(n=3)	(n=3)
Total cholesterol	24 ± 0.8	24 ± 0.8	21 ± 1.6	26	23 ± 0.7	25 ± 2.9
Triglycerides	4.1 ± 1.3	3.4 ± 1.0	4.1 ± 1.1	5.4	2.7 ± 0.7	3.1 ± 0.5
Serum lipid levels (mmol/l) at 6 months old	(n=3)	(n=1)	(n=7)	(n=1)	(n=3)	(n=3)
Total cholesterol	23 ± 3.7	26	28 ± 3.3	32	25 ± 0.3	31 ± 2.8
Triglycerides	2.1 ± 0.7	3.28	2.8 ± 0.5	2.7	2.0 ± 0.5	2.0 ± 1.0
Serum lipid levels (mmol/l) at 12 months old			(n=5)		(n=3)	(n=3)
Total cholesterol			23 ± 2.2		24 ± 3.7	25 ± 1.3
Triglycerides			3.6 ± 0.7		2.5 ± 0.2	2.9 ± 0.8
Serum lipid levels (mmol/l) at 18 months old					(n=3)	(n=3)
Total cholesterol					21 ± 3.2	21 ± 3.2
Triglycerides					2.4 ± 0.8	1.7 ± 0.3
Serum lipid levels (mmol/l) at 24 months old					(n=1)	(n=2)
Total cholesterol					29	22 ± 3.9
Triglycerides					2.4	2.3 ± 0.1
Body weight at sacrifice (kg)	2.8 ± 0.2	2.6 ± 0.3	3.4 ± 0.3	2.8	3.4 ± 0.5	2.9 ± 0.3
Coronary lesions						
Maximum stenosis (%) *	78 ± 18	50 ± 28	76 ± 5	80	88 ± 8	90 ± 9
Average stenosis (%)	31 ± 9	23 ± 12	47 ± 12	44	76 ± 7	78 ± 17
Sections with lesions (%)	58 ± 12	46 ± 4	67 ± 23	60	86 ± 14	86 ± 14

Data are represented as the mean ± SD. Values in parentheses represent number of rabbits analyzed.

\* Maximum stenosis was calculated using the section showing the most severe coronary cross-sectional narrowing for each rabbit.





**Supplemental Fig. 1.** (A) Frequency of sections with lesions of acute angle-type LCX and obtuse angle-type LCX at the main curvature. (B) Cross-sectional narrowing of acute angle-type LCX and obtuse angle-type LCX at the main curvature. In 6 months age group, number of rabbits was 3 in obtuse angle type and 2 in acute angle type. In 12 months old group, it was 5 in obtuse angle-type LCX and 3 in acute angle-type LCX. In 24 months old group, it was 3 in both obtuse angle-type LCX and acute angle-type LCX. Data were represented as the mean  $\pm$  SD. Statistical analyses were performed by Mann-Whitney *U*-test.

**Supplemental Table 2.** Comparison of rabbits with obtuse angle LCX and acute angle LCX

	Obtuse angle-type	LCX Acute angle-type LCX	P-value
Number of rabbits	9	10	
Percentage of sections with lesions (%)	55 $\pm$ 19	81 $\pm$ 18	0.008
Average cross-sectional narrowing (%)	26 $\pm$ 21	51 $\pm$ 26	0.022
Percentage of sections with fibrous lesion (%)	44 $\pm$ 20	27 $\pm$ 15	0.191
Percentage of sections with lipid-rich lesions (%)	32 $\pm$ 31	42 $\pm$ 26	0.305
Serum lipid levels at 6 months-old	(n=8)	(n=10)	
Total cholesterol (mmol/L)	28 $\pm$ 3	27 $\pm$ 5	0.563
Triglyceride (mmol/L)	2.6 $\pm$ 0.7	2.3 $\pm$ 0.7	0.290
Serum lipid levels at 12 months-old	(n=5)	(n=7)	
Total cholesterol (mmol/L)	23 $\pm$ 2	24 $\pm$ 2	0.674
Triglyceride (mmol/L)	3.4 $\pm$ 1.0	2.9 $\pm$ 0.6	0.287

Data are represented as the mean  $\pm$  SD. Statistical analyses were performed by Mann-Whitney *U*-test for atherosclerotic lesions and by Student *t*-test for serum lipid levels.

Serum lipid levels were analyzed using 8 rabbits with obtuse angle LCX and 10 rabbits with acute angle LCX at 6 months old, and 5 rabbits with obtuse angle LCX and 7 rabbits with acute angle-LCX at 12 months old.